Article ID：1007−7294(2026)06−0894−16

# Numerical Simulation Study of Power Output Characteristics of Vertical-Axis Self-starting Power Generators

*JIN Feng*, *HUANG Zhou−yi*

(School of Naval Architecture and Ocean Engineering, Jiangsu University of Science and Technology, Zhenjiang 212003, China)

**Abstract:** To address the difficulty in self-starting for vertical-axis water turbines with fixed pitch angles and to improve the efficiency of marine energy utilization, a hybrid power generation device was proposed that incorporated a Savonius-type wind rotor to assist in starting the vertical-axis water turbine. Numerical simulations were conducted to investigate the dynamic output characteristics of this integrated device. Firstly, a three-dimensional two-phase flow numerical tank was constructed using Fluent software, and the mesh partitioning scheme was determined by comparing the values of the power output parameters of the device under different mesh densities, and at the same time, the validity of the numerical tank was confirmed. Secondly, the established numerical tank was used to simulate the variation law of torque, speed and power coefficient of power generation devices under different flow field conditions with different water wheel blade numbers, radius ratios and height ratios. The results show that the device performs better in terms of torque stability, speed characteristics, and energy utilization in the simulated working condition range when the water wheel blades are 3 to 4, the radius ratio is 0.25 to 0.375, and the height ratio is 1/6 to 1/3. The device is able to start quickly in the presence of wind, and the power coefficient reaches 0.3 to 0.4 or even exceeds 0.4, with good starting and power generation performance. The research results can provide a reference for the design and application of the device.

**Key words: Fluent; vertical-axis power generator; numerical simulation; starting performance; energy utilization characteristics**

**CLC number**：U661.4 **Document code**：A **doi:** 10.3969/j.issn.1007−7294.2026.06.004

## 0 Introduction

Offshore multi-energy integrated power generation has the potential to enhance the utilization rate of marine energy and mitigate the limitations of single-energy power generation. This development aligns with a major trend in the field of marine energy. However, there are challenges associated with this type of power generation device, including a complex and cumbersome structure, low energy conversion efficiency, and high power generation costs. The impeller generator, as the core component of the transducer device, exerts a direct influence on the generator's energy conversion efficiency and the kinetic performance of its structural

Received date：2026−03−13

Foundation items：Supported by the Key Laboratory of Water-Sediment Sciences and Water Disaster Prevention of Hunan Province (2020SS03)

Biography：JIN Feng (1980−), female, Ph.D., associate professor, corresponding author, E-mail: jflook@126.com; HUANG Zhou-yi (2000−), male, master, E-mail: 1939059774@qq.com.

form. The design and optimization of the impeller generator structure have emerged as a focal point of research in various countries, driven by the pursuit of enhanced dynamic performance. The vertical-axis fixed-pitch water turbine for tidal energy, whose blades are fixed on the spokes with a certain angle, functions reliably and efficiently; however, it cannot self-start, which has become its main drawback of this turbine. Conversely, the Savonius-type wind turbine of wind energy exhibits good starting performance and high torque. To address the challenge of the vertical-axis fixed-pitch water turbine's inability to self-start and to leverage the full potential of wind, wave, and tidal energy, this study proposes a novel integrated power generation device. This device involves the installation of a Savonius-type wind turbine on top of the existing vertical-axis water turbine. The large starting torque characteristic of the Savonius-type wind turbine can assist in starting the vertical-axis water turbine, thereby enhancing its functionality and efficiency. This combined power generation device has a simple structure and low cost. It is capable of capturing the scattered, fluctuating, and intermittent energy of wind, waves, and currents. The device combines these energies into high-efficiency mechanical energy. It achieves energy superposition to maximize the use of integrated power generation from ocean energy. This adaptation aligns with the demand for comprehensive utilization of ocean energy and the concept of sustainable development.

In recent years, there has been an increase in research activity focused on single-energy power generators[1−14]. In comparison, there is a paucity of studies on multi-energy integrated power generation devices at home and abroad. Cao[15] analyzed and studied the hydrodynamic characteristics, stability, and strength of a floating power generation platform under the combined action of wind, wave and currents using AQWA software. Ji[16] and Chen[17] designed a wind-wave energy coupled power generation experimental platform and established a Simulink simulation model using MATLAB to investigate the speed and torque characteristics of the power coupling mechanism under the complementary power generation mode. Jing[18] took a vertical-axis three-bladed tidal current turbine as the research object and used CFX software to establish a second-order Stokes wave flume to investigate the hydrodynamic performance changes of the turbine under the combined action of waves and uniform flow. Mojica et al[19] integrated a Darrieus wind turbine and a Savonius wind turbine into a vertical-axis structure and evaluated the performance of the hybrid wind turbine through model tests, concluding that the efficiency of the system is close to 63%. Saini et al[20] improved the poor starting performance of the Darrieus rotor by introducing a hybrid rotor and optimized the structural dimensions using the Fluent numerical simulation method. Wuryanti et al[21] explored the feasibility of a combined system of Savonius drag-type water turbines and propeller lift-type water turbines in seawater current energy conversion, and verified its performance through numerical simulations using Fluent software and physical experiments. Among the various research methods employed in the study of power generating devices, the computer numerical simulation method is of particular significance due to its low investment, short cycle time, and easy modification of various parameters. In numerical simulation methods, MATLAB’s specialized fluid simulation capabilities are relatively weak, AQWA has limitations such as insufficient accuracy for highly nonlinear fluid phenomena, and CFX has high requirements for mesh quality. In contrast, Fluent offers strong mesh compatibility, good adaptability to complex transient problems, and wider applicability in engineering scenarios.

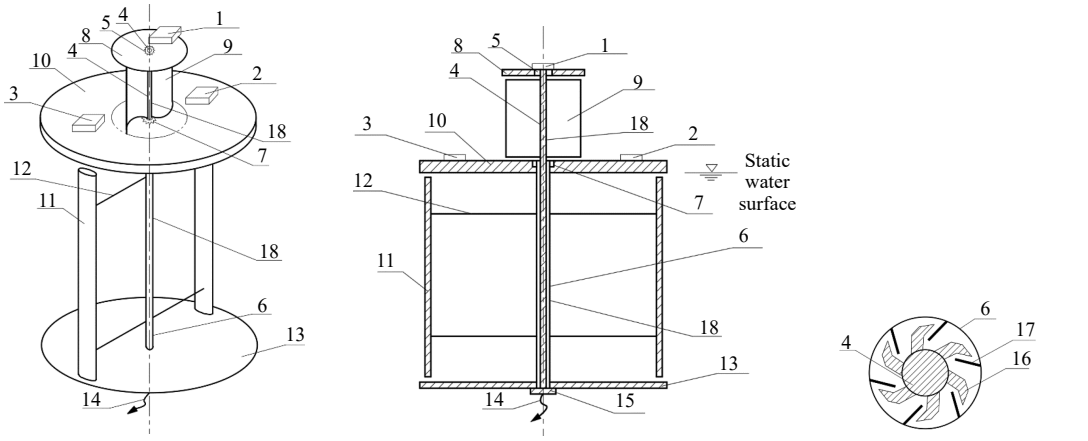
Complementary power generation is a challenging problem involving multiple fields and technologies. It not only requires efficiently harvesting various energy sources and converting them into electrical energy to the maximum extent, but also aims to improve power generation efficiency while reducing costs. Although some progress has been made in related research, many technologies are still in their infancy, which hinders

large-scale development and implementation. The performance of integrated power generation devices in combined environments is extremely complex, and research results in this area remain relatively limited. This is also due to the structure of different devices, which necessitates the exploration of specific devices. In this paper, an offshore multi-energy integrated power generation device is constructed on the basis of a vertical-axis fixed-pitch hydraulic turbine. We propose to establish a three-dimensional numerical tank under the joint environment of wind and current using the Fluent numerical simulation method. The starting and energy output characteristics of the power generation device will be investigated. This will provide a basis and technical support for the design and application of this power generation device, and also offer a certain reference for the development of marine energy complementary power generation technology.

# 1 Generator and power output parameters

### 1.1 Structure of the power generation unit

The lower part of the vertical-axis self-starting integrated power generation device is a fixed-pitch hydraulic turbine, the upper part is a Savonius wind rotor, and the middle part is a circular floating plate on which solar thin-film batteries can be laid. The three-dimensional view and cutaway view of the structure are shown in Fig.1(a)−(b). The device's functionality encompasses the integration of power generation from wind, water, and solar sources. Its starting mechanism is as follows: when the wave and flow forces are small, and the driving torque on the water turbine is less than the static resistance torque of the system, the water turbine will be unable to operate. In this case, the Savonius wind turbine, which features a large torque moment compared to the resistance, can be used for auxiliary starting. That is, the wind turbine rotates under low wind force, thereby driving the connected water turbine to rotate. After the water turbine gains an initial speed, the system state will undergo a fundamental change. During rotation, the stress angle of the water turbine blades is optimized, the torque received increases, and the resistance decreases, ensuring that the driving torque of the water flow always overcomes the resistance torque, ultimately achieving continuous rotation.




（a）Stereogram （b）Cutaway view （c）Overrunning device structure

Fig.1 Schematic diagram of the structure of the integrated power generation unit (1. Wind turbine; 2. Hydroelectric generator; 3. Solar generator; 4. Inner shaft; 5. First transmission gear; 6. Outer shaft; 7. Second transmission gear; 8. Circular flat plate; 9. Savonius blades; 10. Floating plate; 11. Water turbine blades; 12. Connecting rods; 13. Circular base plate; 14. Anchoring equipment; 15. End cap; 16. Beveled gear pattern; 17. Soft bayonet; 18. Vertical axis)

An overrunning device is installed between the outer shaft and the inner shaft of the device, as shown in Fig.1(c). This ensures that during the operation of the device, when the water turbine blades rotate faster than the savonius blades, they will not drive the savonius blades to rotate, so as to guarantee the efficiency of the water turbine. Conversely, when the savonius blades rotate faster, it can further drive the water turbine blades to rotate. On one hand, this can enhance the operation of the water turbine; on the other hand, it is beneficial for overspeed control of the savonius blades.

**1.2 Power output parameters**

The power output parameters of the generator principally comprise the moment ($M$), rotational speed ($\omega$), and power coefficient ($C_P$)[4,9]. Since the hybrid power generation device presented in this paper is primarily based on water turbine power generation, the moment of the water turbine is the main focus here. In fixed-axis rotation, the magnitude of the moment is equal to the product of the force and the force arm. Rotational speed is the number of revolutions or the angle turned by an object in circular motion per unit of time. Assuming that the device is operating in a steady state, if $n$ represents the rotational speed, then the angular velocity $\omega$ is

$$\omega = \frac{\pi n}{30} \tag{1}$$

The power coefficient represents the efficiency with which the device converts the kinetic energy of the fluid into mechanical power, defined as the ratio of the output power $P_{out}$ to the input power $P_{in}$. Here, $P_{in}$ refers to the kinetic energy power extracted by the device from the fluid, i.e., the kinetic energy carried by the fluid as it flows through the effective force-bearing cross-section of the device per unit time[19,21]. For an incompressible fluid, the input power obtained by the device from the wind can be expressed as

$$P_{in1} = \frac{1}{2}\rho_1 A_1 U_1^3 \tag{2}$$

The input power that the device obtains from the water flow can be expressed as

$$P_{in2} = \frac{1}{2}\rho_2 A_2 U_2^3 \tag{3}$$

For the fixed-axis rotating device operating in a steady state, the output power can be expressed as

$$P_{out} = M\omega \tag{4}$$

From the above analysis, it can be seen that when the device is subjected only to wind speed, the power coefficient is given by

$$C_p = \frac{P_{out}}{P_{in1}} = \frac{2M\omega}{\rho_1 A_1 U_1^3} \tag{5}$$

When the device is only affected by the water flow velocity, the power coefficient is

$$C_p = \frac{P_{out}}{P_{in2}} = \frac{2M\omega}{\rho_2 A_2 U_2^3} \tag{6}$$

When the device is simultaneously affected by wind speed and flow velocity, the power coefficient is

$$C_p = \frac{P_{out}}{P_{in1} + P_{in2}} = \frac{2M\omega}{\rho_1 A_1 U_1^3 + \rho_2 A_2 U_2^3} \tag{7}$$

In Eqs.(2)–(7) $P_{in1}$ and $P_{in2}$ are the input powers obtained by the device from the wind and water flow respectively, $\rho_1$ and $\rho_2$ are the densities of air and water, respectively, $A_1$ and $A_2$ are the projected areas of the wind plate and the water turbine on the cross-section perpendicular to the incoming flow, respectively, $U_1$ and $U_2$ are the incoming speeds of the air and water, respectively.

## 2 Parameters of the numerical model of the power generation unit and calculation conditions

The configuration of the integrated power generation unit is intricate; consequently, the model of the unit has been appropriately simplified in the simulation, considering the expected goals and operability. The simplified three-dimensional perspective view of the model is shown in Fig.2. It consists of two main components: the S-type wind rotor and the H-type turbine. In addition, circular thin plates with a slightly larger diameter are installed above and below the S-type wind rotor to increase the wind speed. The model does not consider the overrunning device, and the wind rotor and the turbine are connected coaxially and rotate in unison, while all other components remain stationary.

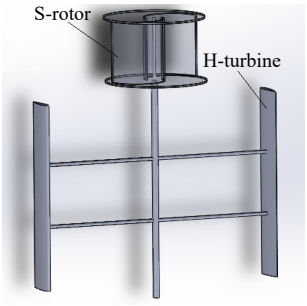


Fig.2 Simplified model of an integrated power generation

The turbine blade of the power generation unit is NACA0018 wing type, with a blade chord length of 0.6 m, a turbine diameter of 0.8 m, and a height of 0.6 m. The main research parameters include the number of turbine blades, the relative radius ratio of the structure, and the relative height ratio of the structure, the wind speed, and the flow speed. The number of turbine blades is in three cases: 2, 3, and 4. The structure relative radius ratio is the ratio of the radius of the wind rotor to that of the water turbine, which are 0.25, 0.375 and 0.5, respectively. The structure relative height ratio is defined as the ratio of the height of the wind rotor and the water turbine, with values of 1/6, 1/3, and 1/2, respectively. Considering the typical ranges of wind and flow velocities commonly encountered in engineering practice, wind speeds of 1 m/s and 2.5 m/s, and flow velocities of 0.35 m/s and 0.5 m/s are selected to represent low and moderate levels, respectively. There are 21 distinct working conditions.

## 3 Establishment of a three-dimensional numerical tank

### 3.1 Control equation

Considering that the interaction between this power generation device and wind and water flow is unsteady, the continuity equation and N-S equation are used for the control equations in the numerical calculations, the turbulence model is closed by the $k-\varepsilon$ model, the free liquid surface is tracked by the VOF multiphase flow model, and the bidirectional interactions between the fluid and the moving objects are restored by the dynamic mesh 6DOF model [5,10].

### 3.2 Three-dimensional numerical tank parameters

The dimensions of the three-dimensional numerical tank are: length 8 m, width 3 m, and height 2 m. The computational domain is illustrated in Fig.3[6,8]. The left side of the tank is configured as the air inlet and the water inlet, both of which are designated as velocity inlets with a static water surface height of 1.22 m. The right side of the pool is designated as the pressure outlet, and the surrounding walls are configured as the symmetry boundary conditions, indicating an infinitely large space. To facilitate the simulation of the flow field, the computational domain of the numerical tank is divided into two parts: the stationary domain and the rotating domain. The rotating domain is a cylinder with a diameter of 1 m and a height of 1 m. The outside of

the rotating domain is the stationary domain, and the boundary between the rotating domain and the stationary domain is the internal boundary which allows the free flow of fluid. The center of the rotating domain is positioned at a distance of 2 m from the velocity inlet, 1.5 m from the two walls in the width direction, 1.105 m from the top of the computational domain, and 0.895 m from the bottom of the computational domain. The power generation unit is situated within the rotating domain and is coaxial with the rotating domain. The top of the turbine blades is positioned at a distance of 0.025 m from the static surface of the water, and the bottom of the wind plate is positioned at a distance of 0.025 m from the static surface of the water.

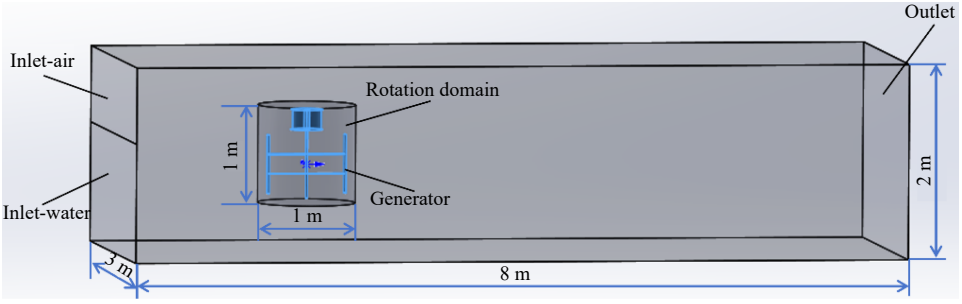



Fig.3 Schematic diagram of the computational domain of a 3D numerical tank

### 3.3 Numerical tank grid settings

The results of the numerical tank calculation domain meshing are shown in Fig.4 and 5. The computational domain includes a stationary domain, a rotating domain and the power generator. The specific corresponding cell sizes of each domain are shown in Tab.1[4].

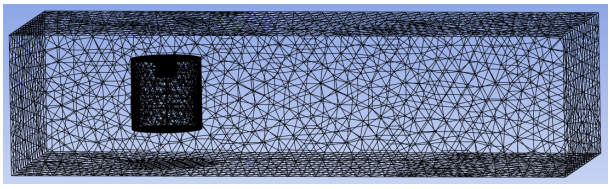


Fig.4 Computational domain grid

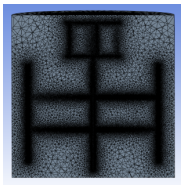


Fig.5 Rotation domain grid

**Tab.1 Corresponding cell sizes of each domain**

| Grid number | The cell size of the wall of the power generator/mm | The cell size of the rotating zone/mm | The cell size of the stationary zone/mm | Grid number | The cell size of the wall of the power generator/mm | The cell size of the rotating zone/mm | The cell size of the stationary zone/mm |
|---|---|---|---|---|---|---|---|
| 1 | 7 | 175 | 350 | 3 | 5 | 125 | 250 |
| 2 | 6 | 150 | 300 | 4 | 4 | 100 | 200 |

The simulated flow field is relatively complex, and the boundary layer thickness exhibits non-uniform distribution and local fluctuations. Therefore, the Scalable Wall Function is employed to avoid numerical divergence. To enhance convergence efficiency and stability, the Coupled Algorithm is used for solving the N-S equations. The PRESTO scheme is adopted for pressure interpolation to accommodate scenarios with significant pressure variations in turbulent flows.The Least Squares Cell-Based method is used for gradient calculation; the Second-Order Upwind Scheme is applied to the dynamic equation of turbulent kinetic energy; and the residual threshold is set to $1.0\times10^{-4}$. The density of air is 1.225 kg/m$^3$, and its viscosity is $1.7894\times10^{-5}$ kg/ (m·s). The density of water is 998.2 kg/m$^3$, and its viscosity is $1.003\times10^{-3}$ kg/ (m·s).

### 3.4 Grid-independent verification

In this instance, the simulation is conducted for a power generation unit with a turbine blade number of 3, a structure relative radius of 0.375, and a relative height of 1/3 under wind speeds of 1 m/s and flow velocities of 0.35 m/s. Through simulation calculation and monitoring, the overall torque and rotational speed of the device are obtained, and then the power coefficient under the simultaneous action of wind and flow is calculated using Eq.(7). In accordance with the range of cell sizes delineated in subsection 3.3, four grid quantities, 1 562 597, 2 006 876, 2 633 941, and 3 743 968, are selected for the grid-independence validation. The computed rotational speeds and power coefficients are presented in Tab.2.

**Tab.2 Mesh-independence calculation results**

| Grid number | Number of grids | Rotational speed $\omega$/(rad·s$^{-1}$) | Power coefficient $C_p$ | Grid number | Number of grids | Rotational speed $\omega$/(rad·s$^{-1}$) | Power coefficient $C_p$ |
|---|---|---|---|---|---|---|---|
| 1 | 1 562 597 | 2.082 | 0.328 | 3 | 2 633 941 | 2.241 | 0.358 |
| 2 | 2 006 876 | 2.184 | 0.346 | 4 | 3 743 968 | 2.272 | 0.364 |

As illustrated in Tab.2, the number of grids increases from 1 562 597 to 3 743 968 in a proportionate and gradual manner. The rotational speeds between neighboring grids exhibit errors of 4.9%, 2.6%, and 1.4%, respectively, while the errors between neighboring power coefficients are 5.6%, 3.2%, and 1.8%, with errors gradually converging. The discrepancy between the power coefficients is marginally more pronounced than that observed between the rotational speeds. This discrepancy can be attributed to the fact that the power coefficient is a composite parameter calculated from the torque and rotational speed. The superposition of the errors of these two parameters results in a larger error in the power coefficient. The error data reveal that the grid calculation results of cases 3 and 4 are more similar, indicating that the number of grids can meet the calculation requirements[4,13]. In this instance, the case 4 is selected for subsequent study: the grid cell size of the rotating domain and its interface is 100 mm, the wall grid cell size of the power generation device is 4 mm, and the fluid domain grid cell size outside the rotating domain is 200 mm. At this point, the average grid skewness is 0.228 66, the maximum grid skewness is 0.895 74, the average orthogonal quality is 0.769 93, and the average element aspect ratio is 1.8454. Overall, the grid skewness is relatively small, the orthogonal quality is high, and the aspect ratio is reasonably distributed, indicating that the grid cells are relatively regular in shape. All grid quality metrics are within acceptable ranges and can satisfy the requirements for grid accuracy and stability in the numerical simulations presented in this paper.

## 4 Numerical simulation of power output characteristics

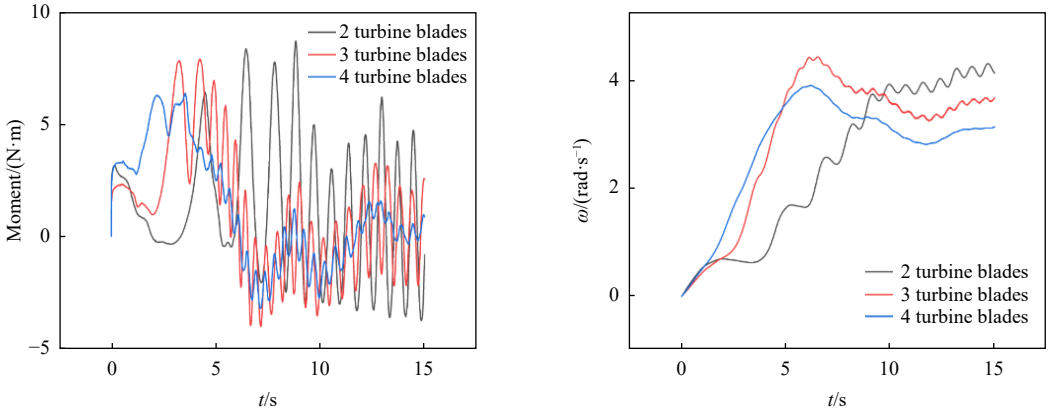
### 4.1 Start-up performance

4.1.1 Influence of the turbine blades number

(1) Water flow rate effect

The results of the torque and rotational speed changes during the power generator's starting process are shown in Fig.6 for a given water flow rate of 0.5 m/s. The fluctuations in torque and rotational speed over time manifest a discernible regularity, primarily during the adjustment phase before 8 s and the subsequent stabilization phase. It is evident that with an increase in the blade number, the torque fluctuation decreases, leading to enhanced stability. However, the rotational speed attains a stable value that exhibits a downward trend with an increase in the blades number. This phenomenon can be attributed to the fact that when the blade number is the smallest, the device's weight is relatively small, and it is more susceptible to external

environmental influences, resulting in greater fluctuations in the curve. In general, when the blade number is 3 or 4, the torque stability is enhanced, the rotational speed is more uniform, the curve fluctuation is reduced, and the device is less susceptible to external environmental influences.

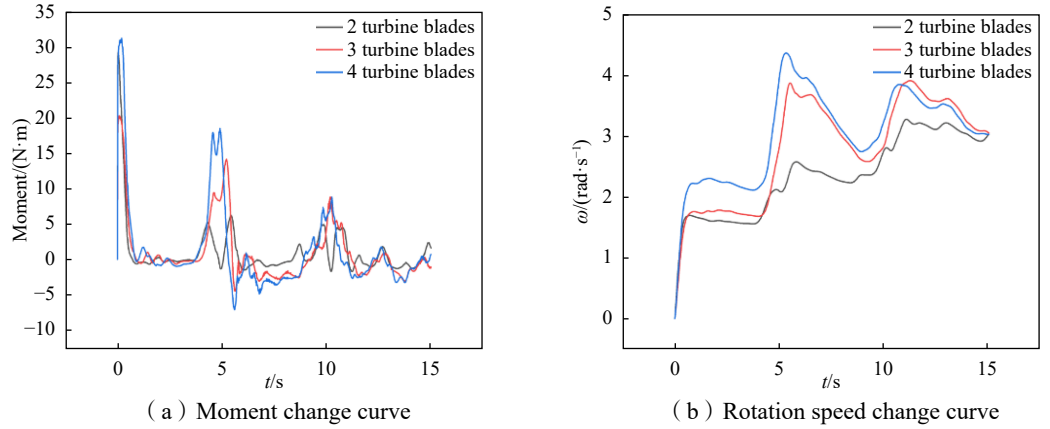



（a）Moment change curve　　（b）Rotation speed change curve

Fig.6 Change curve of torque and rotation speed when the water flow rate is 0.5 m/s

(2) Wind speed effect

At a given wind speed of 2.5 m/s, the results of the torque and speed variations during the starting process of the power generator are shown in Fig.7. It can be seen that both torque and speed gradually stabilize after three successive peaks. As the blade number increases, the fluctuation amplitude of torque and speed tends to increase, which is different from the fluctuation characteristics of the combined generating unit under the influence of flow rate only. It is considered that when the turbine has a large number of blades, the water turbine blades themselves are not directly affected by the wind speed. However, the force on the wind rotor blades affected by the wind speed will be transferred to the turbine. At this time, the moment of inertia of the turbine is relatively large, which makes the response of the whole device relatively sluggish, leading to the larger fluctuation amplitude of torque and speed. When the blade number is 2 or 3, the torque and rotational speed are more stable, and the adaptability to the change of wind speed is better, which cannot only reduce the mechanical impact and loss of the device due to the large operating amplitude, but also ensure the stable output of energy to a certain extent.



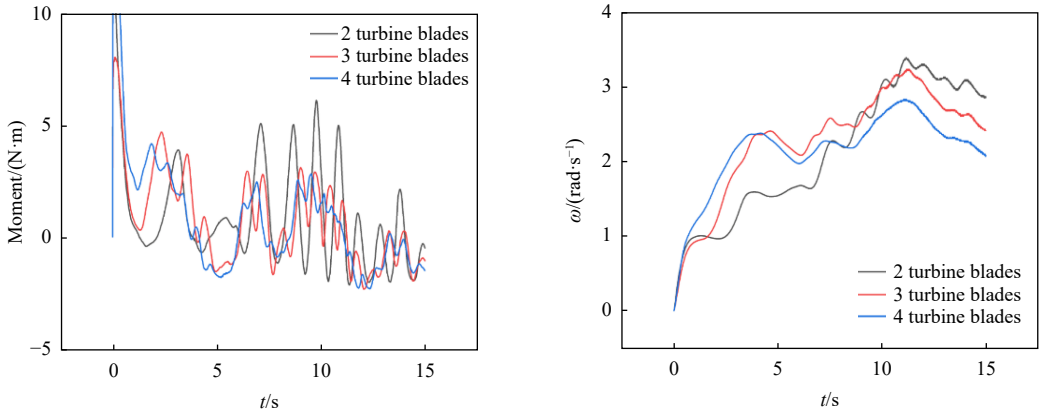

（a）Moment change curve　　（b）Rotation speed change curve

Fig.7 Change curve of torque and rotation speed when the wind speed is 2.5 m/s

(3) Simultaneous action of wind speed and water flow rate

At a given wind speed of 1 m/s and water flow rate of 0.35 m/s, the results of torque and speed changes during the starting process of the power generator are shown in Fig.8. Both torque and speed curves

experience rapid rise and fall in the early stage, and gradually stabilize after about 8 s. In the stabilization stage, when the blade number is 2, the weight of the device is small and sensitive to environmental changes, which makes the curve fluctuate more frequently and with a larger amplitude; when the blade number is 3 or 4, the curves are closer to each other, especially when the blade number is 3, the fluctuation of the torque is relatively flat and the speed is larger at the same time, which is able to better balance the energy output and the stability of the device operation.



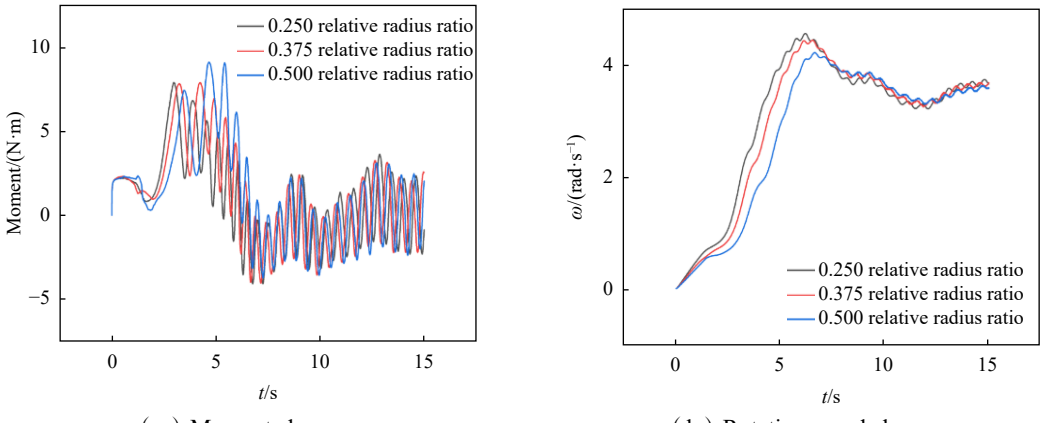

（a）Moment change curve （b）Rotation speed change curve

Fig.8 Change curve of torque and rotation speed when the wind speed is 1 m/s and water flow rate is 0.35 m/s

4.1.2 Influence of relative radius ratios

(1) Water flow rate effect

The results of torque and speed changes during the starting process of the power generator are shown in Fig.9. It can be seen that the effect of changing the radius ratio on the torque and speed is small, and the curves are relatively close to each other. The curves basically fluctuate before 8 s, the larger the radius ratio is, the greater the fluctuation of the torque value is and the slower the speed increases, and the curves stabilize after 8 s. The larger the radius ratio is, the larger the wind rotor is relative to the turbine, and the larger the rotational inertia of the whole device is, which makes it more difficult to adjust the motion state of the device, leading to obvious torque fluctuation and slower speed increase.



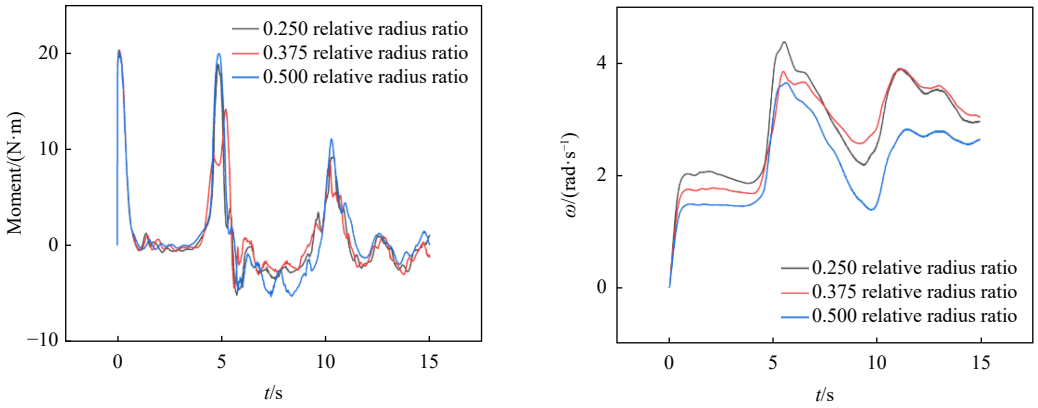

（a）Moment change curve （b）Rotation speed change curve

Fig.9 Change curve of torque and rotation speed when the water flow rate is 0.5 m/s

(2) Wind speed effect

The results of the torque and speed changes during the starting process of the power generator are shown in Fig.10. The torque and speed are basically in the adjustment stage before 12 s, both of which have three

peaks, and gradually stabilize after 12 s. The curves with radius ratios of 0.25 and 0.375 are relatively close to each other, while the torque fluctuation is larger when the radius ratio is 0.5, and the speed curves also deviate and the speed values are smaller, which is related to the larger weight of the device when the radius ratio is large.

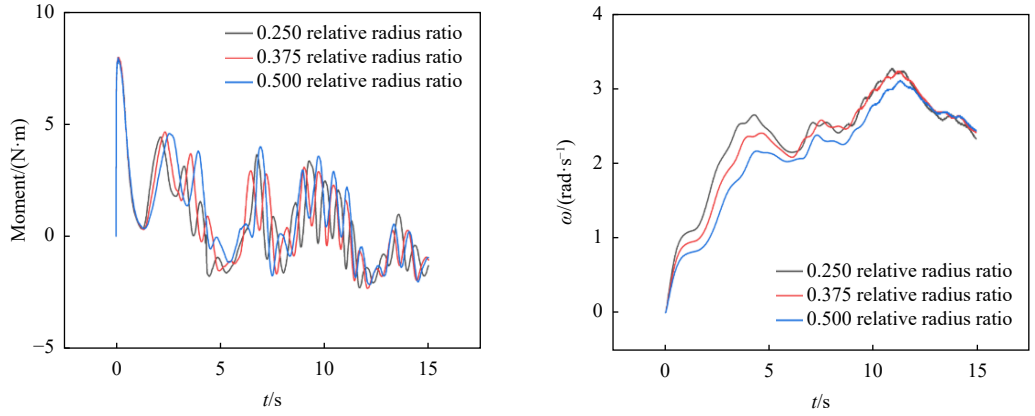



（a）Moment change curve　　（b）Rotation speed change curve

Fig.10 Change curve of torque and rotation speed when the wind speed is 2.5 m/s

(3) Simultaneous action of wind speed and water flow rate

The results of the torque and speed variation during the starting process of the power generation unit are shown in Fig.11. From the figure, it can be seen that approximately before 12 s is the starting adjustment stage, and after 12 s the device operation enters the stabilization stage. The curves with radius ratios of 0.25 and 0.375 are closer to each other, and the curve with radius ratio of 0.5 is slightly different. The larger the radius ratio, the greater the torque fluctuation and the slower the speed increase.




（a）Moment change curve　　（b）Rotation speed change curve

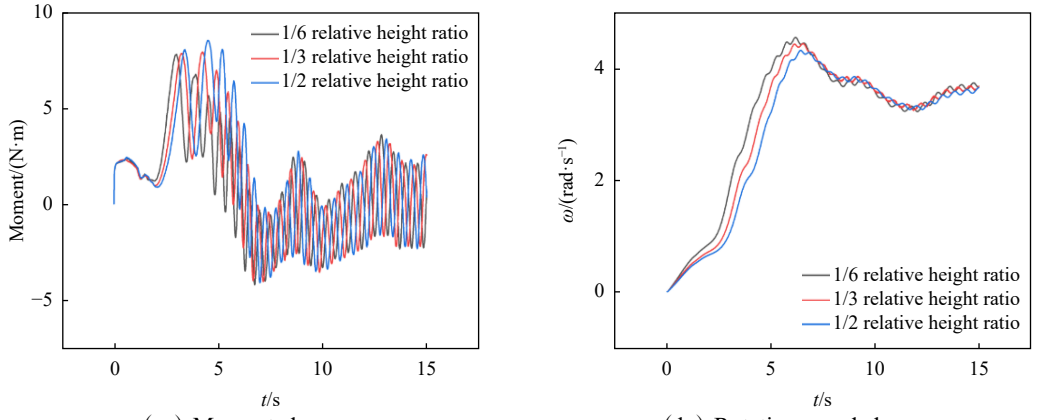
Fig.11 Change curve of torque and rotation speed when the wind speed is 1 m/s and water flow rate is 0.35 m/s

4.1.3 Influence of relative height ratios

(1) Water flow rate effect

The results of the torque and speed changes during the starting process of the device are shown in Fig.12. It can be seen that the height ratio has a certain effect on the torque and speed before 7 s: the larger height ratio leads to greater torque fluctuation and speed increase. After 7 s, the height ratio basically has no effect on the torque and speed changes; the curves roughly overlap and follow a uniform trend. When the height ratio is 1/3 and 1/6, the relative position of the wind rotor is low, the center of gravity of the device is low, the rotational moment of inertia is small, the structure is compact and rigid, and it is less affected by the

changes of the water flow field.

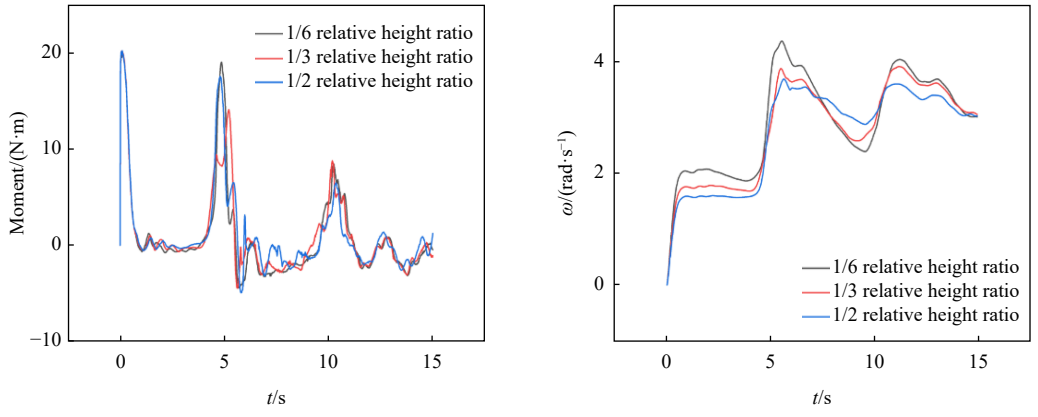



（a）Moment change curve （b）Rotation speed change curve

Fig.12 Change curve of torque and rotation speed when the water flow rate is 0.5 m/s

(2) Wind speed effect

The results of the torque and speed change during the starting process of the power generator are shown in Fig.13. From the figure, it can be seen that both the torque and speed curves are gradually stabilized after reaching three peaks, i.e., the curves are more consistent and smooth after 12 s. The wind rotor with large height ratio has a large wind area and captures more wind energy; the initial torque is high and rises quickly; but the vibration and deformation of the device structure are also greater, leading to more drastic torque fluctuation. Comparatively, the fluctuation amplitude of the torque is smaller and the peak value is slightly lower when the height ratio is 1/3 or 1/6, and the fluctuation amplitude and peak value of the rotational speed under the height ratios of 1/3 and 1/2 are close to each other, which indicates that under the effect of wind speed, the device with the height ratio of 1/3 can better utilize the wind energy and avoid the unstable operation of the device and the increase of wear of the components due to the fluctuation amplitude at the same time, while obtaining the higher rotational speed.



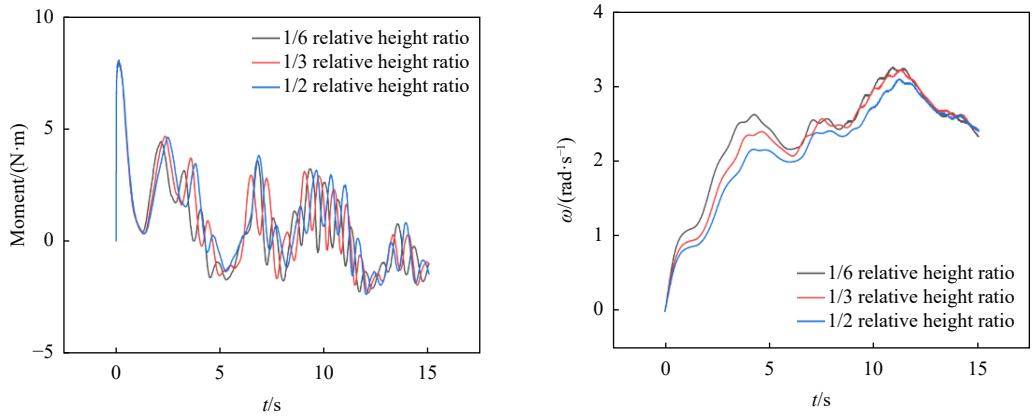

（a）Moment change curve （b）Rotation speed change curve

Fig.13 Change curve of torque and rotation speed when the wind speed is 2.5 m/s

(3) Simultaneous action of wind speed and water flow rate

The results of the torque and speed change during the starting process of the device are shown in Fig.14. It can be seen that under the combined effect of wind and current, the change of the height ratio of the device does not have a significant effect on the torque and rotational speed, the curves are relatively close and the trend of change is basically the same, and the device operation enters a stable stage around 12 s. When the

height ratio is 1/2, the torque fluctuation is greater, the peak value is higher, and the rotational speed grows more slowly, which is related to the fact that the device with a large height ratio is easily vibrated and deformed under the joint action, which affects the energy transmission and other factors.




（a）Moment change curve　　（b）Rotation speed change curve

Fig.14 Change curve of torque and rotation speed when the wind speed is 1 m/s and water flow rate is 0.35 m/s

Overall, under the combined effect of wind and current, the integrated power generation device shows a rapid increase in torque and speed during the initial starting phase, reaching a certain speed within 1 s. While under only flow conditions, the device starting time is longer, indicating that the device through the addition of the wind rotor to improve the turbine starting performance of the design concept is more reasonable.

**4.2 Energy utilization characteristics**

4.2.1 Effect of the turbine blade number on energy utilization characteristics

(1) Water flow rate effect

The calculation results of the corresponding power coefficient of the power generation device at the given water flow rate of 0.5 m/s are shown in Tab.3. It can be seen that under the effect of flow rate, the power coefficients for 2 and 4 blades are similar, and the power coefficient of the power generation device is larger when the blade number is 3, resulting in a higher energy utilization rate. It is believed that when the blade number is 3, the flow field synergy between the blades is better, which is conducive to energy harvesting, and the rotating torque of the device is larger, which improves the energy utilization and makes the power coefficient larger.

**Tab.3 Effect of various parameters on power coefficient $C_p$**

| Parameters | Parameter values | $C_p$ (water flow rate 0.5 m/s) | $C_p$ (wind speed 1 m/s, water flow rate 0.35 m/s) |
|---|---|---|---|
| Number of turbine blades | 2 | 0.200 | 0.344 |
| | 3 | 0.234 | 0.364 |
| | 4 | 0.201 | 0.383 |
| Relative radius ratios | 0.25 | 0.225 | 0.366 |
| | 0.375 | 0.234 | 0.364 |
| | 0.5 | 0.230 | 0.342 |
| Relative height ratios | 1/6 | 0.237 | 0.365 |
| | 1/3 | 0.234 | 0.364 |
| | 1/2 | 0.227 | 0.334 |

(2) Simultaneous action of wind speed and water flow rate

When the given wind speed is 1 m/s and the water flow velocity is 0.35 m/s, the calculation results of

the power coefficient corresponding to the power generation device are shown in Tab.3. The more blades the device has under combined wind speed and flow conditions, the greater the power coefficient and the higher the energy utilization tate. At this time, the change rule of the power coefficient is different from that under flow-only conditions. This is because under the simultaneous action of wind and flow, multiple energy superposition, involving more complex factors, the blade number can increase the swept area, promote synergy with the flow field, improve the energy transfer, which improves the energy utilization rate.

4.2.2 Effect of relative radius ratios on energy utilization characteristics

(1) Water flow rate effect

The calculation results of the power coefficient of the device are shown in Tab.3, indicating that the power coefficients of different radius ratios do not differ much, and the power coefficient of the power generation device at the radius ratio of 0.375 is slightly larger, with a slightly higher energy utilization rate. It is believed that under the radius ratio of 0.375, the distribution of flow field around the turbine blades is more reasonable, and the force of water flow on the blades is more effective, which transmits more momentum, reduces energy loss, and improves energy conversion efficiency.

(2) Simultaneous action of wind speed and water flow rate

The corresponding power coefficients of the device are presented in Tab.3. When the radius ratio is 0.25 and 0.375, the power coefficients of the power generation device are similar and relatively high under the combined effect of wind and water flow. When the radius ratio is 0.5, the wind rotor and the turbine are generally matched in size, resulting in mutual interference and energy loss, and the efficiency of energy capture is low.

4.2.3 Effect of relative height ratios on energy utilization characteristics

(1) Water flow rate effect

The calculation results of the corresponding power coefficients of the device are shown in Tab.3, and it can be seen that the power coefficients are closer when the height ratio is 1/6 or 1/3. The smaller the height ratio, the larger the power coefficient of the power generation device under the effect of flow velocity. This is because a smaller height ratio corresponds to a lower center of gravity and lighter overall weight for the device. Under water flow excitation, such a structure suffers weaker vibration, operates smoothly with lower energy loss, and thereby achieves a higher power coefficient.

(2) Simultaneous action of wind speed and water flow rate

The corresponding power coefficient calculation results are shown in Tab.3. When the height ratio is 1/6 or 1/3, the power coefficients of the power generation device are closer and higher under the simultaneous action of wind speed and flow velocity. When the height ratio is 1/2, the vertical arrangement of the wind rotor and the turbine is poor, causing interference between the wind and water flow fields, and the energy loss increases, resulting in a lower efficiency of the device in capturing energy and an overall power coefficient.

A comprehensive analysis of the available power coefficient data reveals that the power coefficients of the power generation device under a single flow rate range from 0.2 to 0.25, and the power coefficients under the combined action of wind and current range from 0.3 to 0.4, with the latter exhibiting a significant increase over the former. This finding suggests that the device is capable of adapting to its actual application environment, capturing wind and water flow energy and achieving energy superposition, thus enhancing the overall power generation coefficient. The numerical simulation of the device has been simplified, assuming that the wind rotor rotates coaxially with the turbine. In this configuration, the wind rotor will be driven to rotate when the water turbine blades rotate faster than the wind rotor. This will reduce the power generation

efficiency of the turbine due to the drive of the wind rotor to rotate. This indicates that the power coefficient value of the actual structure of the device will be greater, even more than 0.4, which shows that the device has better power generation performance.

## 5 Conclusions

In the present paper, a three-dimensional two-phase flow numerical tank was constructed based on the Fluent numerical simulation method. The research was conducted on the power output characteristics of the vertical-axis self-starting integrated power generator in the wind-water flow combined environment. The main conclusions are as follows

(1) The established numerical tank has been verified to be capable of effectively performing the numerical simulations of the power generation device. A comparison of the difference values of the power output parameters of the device under different grid densities yielded an optimal grid division scheme. The grid cell size of the rotating domain and the interface of the rotating domain is 100 mm, the grid cell size of the wall surface of the power generation device is 4 mm, and the grid cell size of the stationary domain is 200 mm.

(2) The torque and rotational speed variation laws of the power generation device were obtained for different flow fields blade numbers, radius ratios, and height ratios, as well as the variation law of rotational speed. Within the range of simulated conditions, it is suggested that a more rational configuration consists of 3-4 water turbine blades, a radius ratio of 0.25-0.375 between the wind rotor and the turbine, and a height ratio of 1/6-1/3 between the wind rotor and the turbine.

(3) The power coefficient characteristics were obtained for different flow fields blade numbers, radius ratios, and height ratios are given. The power coefficient of the power generation device is observed to be generally larger when the number of blades is 3, the radius ratio is 0.375, and the height ratio is smaller. Under combined wind-flow conditions, an increase in the blade number leads to an increase in the power coefficient. Furthermore, the power coefficient of the power generation device is higher and shows little variation when the radius ratio is 0.25-0.375 and the height ratio is 1/6-1/3.

(4) The rationality of the structural design and application effectiveness of the power generation device were verified. The device demonstrated the capability to initiate operation promptly in the presence of wind, exhibiting satisfactory starting performance. The power coefficient attained under the combined effect of wind flow ranged from 0.3 to 0.4, with the capacity to exceed 0.4. This suggests a high degree of adaptability to environmental conditions and effective power generation performance, indicating a promising trajectory for future development.

### References

[1] Guan Y M, Li X L, Miao Y N, et al. Numerical simulation and wind tunnel test of high-efficiency breeze power generation device[J]. Mechanical Design and Manufacturing, 2022(4): 126–130.

[2] Liu Q. Analysis of energy conversion performance of pipeline-type Savonius hydraulic turbine power plant[D]. Lanzhou University of Technology, 2023.

[3] Liu H, Ding C L, Shi L, et al. Simulation of hydrodynamic characteristics of a new tidal energy generator[J]. Renewable Energy, 2023, 41(3): 420–426.

[4] Zhao H X. Study on the starting process and performance optimization of drag type hydro rotor[D]. Zhenjiang: Jiangsu

University, 2021.

[5] Li Q, Zhao L, Zhang J, et al. Structural optimization design of new Senegal type vertical axis wind turbine[J]. Journal of Hebei University of Science and Technology, 2024, 45(6): 609–617.

[6] Wang S Q. Study on aerodynamic characteristics and flow field of coaxial reversing vertical axis wind turbine blade[D]. Jilin: Northeast Electric Power University, 2023.

[7] Guo Y B. Study on the aerodynamic characteristics of Savonius vertical axis wind turbine with spiral blades[D]. Qinhuangdao: Hebei Science and Technology Normal College, 2022.

[8] Chen W P, Liu Y C, Chen L W. Research on passive rotating hydrodynamic performance of horizontal axis tidal energy turbine based on UDF[J]. Ocean Engineering, 2018, 36(2): 119–126.

[9] Bian P X. Hybrid vertical axis tidal energy hydraulic turbine hydrodynamic performance research[D]. Ji’nan: Shandong University, 2018.

[10] Yang M. Dynamic characteristics and correlation analysis of low-flow impeller with different media[D]. Hohhot: Inner Mongolia Agricultural University, 2023.

[11] Wu Y Z. Analysis and control of dynamic characteristics of variable deflection angle vertical axis tidal energy hydraulic turbine[D]. Harbin: Harbin Engineering University, 2023.

[12] Lv J Z. Hydrodynamic performance of Savonius hydraulic turbine at near free liquid surface and near wall surface[D]. Qingdao: Qingdao University of Science and Technology, 2023.

[13] Li Z, Liu M J, Cao X, et al. Aerodynamic performance analysis and power generation characteristics experiment of vertical axis wind turbine[J]. Engineering Reports, 2022, 4(4): e12500.

[14] Kavade R, Sonekar M, Choudhari D, et al. Investigation on fixed pitch Darrieus vertical axis wind turbine[J], AIP Advances 14, 2024, doi: 10.1063/5.0203609.

[15] Cao M M. Hydrodynamic characterization and stability and strength analysis of floating power generation platform under the combined action of wind and wave currents[D]. Hefei: Hefei University of Technology, 2016.

[16] Ji D H. Research on offshore wind and wave energy coupled complementary power generation platform[D]. Qingdao: Shandong University of Science and Technology, 2017.

[17] Chen G Q. Research on power coupling mechanism of wind and wave complementary power generation platform[J]. Modern Manufacturing Engineering, 2018(1): 146–150.

[18] Jing X X. Effect of wave-current joint action on the hydraulic performance of vertical axis hydraulic turbine[D]. Xi'an: Xi'an University of Technology, 2019.

[19] Mojica E E , Fabay M C , Kehinde F , et al. Design and development of integrated savonius and darrieus small scale vertical axis wind turbine for power generation[J]. IOP Conference Series: Earth and Environmental Science, 2019, 291(1): 012041 (7pp).

[20] Saini G, De A. On the self-starting comparative performance evaluation of Darrieus and hybrid hydrokinetic rotor[J]. International Journal of Energy for a Clean Environment, 2023, 24(5): 67–91.

[21] Wuryanti S, Sasono T, Manunggal B P, et al. Simulation and experimentation of Propeller-Savonius turbine tested underwater surface[J]. Clean Energy, 2024, 8(3): 20–33.

# 垂直轴自起动发电装置动力输出特性模拟研究

金　凤, 黄周裔
（江苏科技大学 船舶与海洋工程学院, 江苏 镇江 212003）

**摘要:** 为解决固定偏角垂直轴水轮机自起动困难的问题, 并提高海洋能源的利用效率, 本文提出了一种集成萨沃纽斯型风轮以辅助垂直轴水轮机起动的综合发电装置。通过数值模拟方法研究了该集成装置的动力输出特性。首先, 采用 Fluent 软件构建了三维两相流数值水池, 通过比较不同网格密度下装置动力输出参数的差异, 确定网格划分方案, 同时验证数值水池的有效性。其次, 利用建立的数值水池, 模拟不同水轮叶片数量、半径比、高度比情况下发电装置在不同流场条件下的力矩、转速和功率系数的变化规律。结果表明, 在模拟工况范围内, 水轮叶片数为 3~4 个、半径比为 0.25~0.375、高度比为 1/6~1/3 时, 装置在力矩稳定性、转速特性及能量利用率方面表现较优。装置能够在有风的情况下迅速起动, 功率系数达到 0.3~0.4, 甚至有望超过 0.4, 起动和发电性能良好。研究成果可为该装置的设计与应用提供参考。

**关键词:** Fluent; 垂直轴发电装置; 数值模拟; 起动性能; 能量利用特性
**中图分类号:** U661.4　　**文献标识码:** A
**基金项目:** 湖南省水沙科学与水灾害防治重点实验室资助项目(2020SS03)
**作者简介:** 金　凤(1980−), 女, 博士, 副教授, 通讯作者, E-mail: jflook@126.com;
黄周裔(2000−), 男, 硕士, E-mail: 1939059774@qq.com。